INSTITUTE OF PHYSICS PUBLISHING JOURNAL OF PHYSICS B: ATOMIC, MOLECULAR AND OPTICAL PHYSICS

J. Phys. B: At. Mol. Opt. Phys. **35** (2002) 2515–2524 PII: S0953-4075(02)31917-5

Absolute cross sections for charge-exchange in $^3He^{2+}$ and H^+ impact on CO

I Čadež[1,2], J B Greenwood[3], A Chutjian[1], R J Mawhorter[1,4], S J Smith[1] and M Niimura[1]

[1] Jet Propulsion Laboratory, California Institute of Technology, Pasadena, CA 91109, USA
[2] Jožef Stefan Institute, SI-1000 Ljubljana, Slovenia
[3] Physics Department, The Queen's University, Belfast, BT7 1NN, UK
[4] Department of Physics and Astronomy, Pomona College, Claremont, CA 91711, USA

Received 13 December 2001, in final form 11 April 2002
Published 24 May 2002
Online at stacks.iop.org/JPhysB/35/2515

Abstract

We report measured absolute single and double charge-exchange cross sections for $^3He^{2+}$ on CO at ion impact energies between 1 and 14 keV (velocities between 254 and 949 km s^{-1}). A retarding-field method is used for charge-state analysis of the ion beam after traversing the target gas cell. Cross sections are determined from absolute measurements of current ratios and the CO target gas pressure. For testing the experimental technique, proton–electron capture cross sections are measured at energies between 2.5 and 7 keV. The measured He^{2+} and H^+ cross sections are compared to available data.

1. Introduction

Protons and He^{2+} ions are the primary ion constituents of the solar wind. The He^{2+} number density varies with time, and can be <1 to 35% of the proton density. All other heavier ions represent only about 0.1% of the solar wind composition. In addition, the energy of He^{2+} also varies with solar activity, so that these ions are important projectiles when diagnostic photon emission from distant objects is observed. In order to model this emission from bodies exposed to the solar wind (e.g., comets and planetary upper atmospheres) absolute cross sections are needed for each incident solar-wind ion and charge state. Recently measured He^+ emission from the comet Hyakutake (Krasnopolsky and Mumma 2001) has prompted us to measure absolute charge-exchange cross section for He^{2+} collisions with CO, since CO is one of the major constituents of the comet's neutral atmosphere near the Sun. As its ionization potential is large (14.0139 eV, or 884.73 Å) solar photoionization rates are low and charge exchange in collisions of solar-wind H^+ ions with CO is the main mechanism for production of CO^+. These ions survive into the tail, scatter solar blue light, and give rise to the characteristic comet tail bands (Magnani and A'Hearn 1986). Collisions of solar-wind He^{2+} with CO also contribute to CO^+ production.

In He^{2+}–CO collisions different processes can occur, and in general one can write

$$He^{2+} + CO \rightarrow He^{(2-j)+*} + CO^{(j+s)+*} + se \tag{1}$$

where $j = 0$, 1 or 2 and $s \geqslant 0$. For $s = 0$ (no free electrons produced by the collision) and $j \neq 0$ one has pure electron capture (charge transfer); for $j = 0$ and $s > 0$ one has ion-impact ionization; and for $j = 1$ or 2 and $s > 0$ one has transfer ionization. In the present experiment we determine absolute charge-changing cross sections. This is the sum of cross sections for all channels with $j = 1$ ($\sigma_{2,1}$, or single charge-exchange) and with $j = 2$ ($\sigma_{2,0}$, or double charge-exchange). In equation (1) only the initial step of the process is indicated. Once $CO^{(j+s)+*}$ is formed it can exit through other channels, including dissociation.

Absolute charge-exchange cross sections have been reported for many different ion–atom and ion–molecule combinations. Nevertheless, when data are needed for a specific application it often appears that new measurements are needed: either the relevant collision partners have not been studied or the appropriate energy range has not been covered. Absolute cross sections for He^{2+}/CO charge exchange were measured by Rudd *et al* (1985) in the energy range between 5 and 150 keV u^{-1}, and more recently by Ishii *et al* (1999) in the low-energy region, from 0.3 to 1333 eV u^{-1}. Our present measurements, which cover 0.333–4.667 keV u^{-1}, fill the energy gap between these two sets of data. They also cover the range of solar-wind velocity of about 1 keV u^{-1} for the solar wind emitted at low heliographic latitudes, to about 4 keV u^{-1} for winds originating in coronal holes (Schawdron and Cravens 2000). Thermal-energy reaction rates of He^{2+} in different gases (including CO) were studied by Tosh and Johnsen (1993).

Important information on ion–molecule collisions lies in determining the final state(s) of the target after collision. Shah and Gilbody (1990) determined relative contributions of dissociative and nondissociative channels in electron capture, transfer ionization and direct ionization in the He^{2+}–CO system. These relative cross sections were normalized in the energy range 6.7–65 keV u^{-1} to the absolute data of Rudd *et al*. This study of Shah and Gilbody was partially motivated by the need for better understanding of solar wind interaction with cometary atmospheres. A detailed study of dissociative fragmentation was carried out by Folkerts *et al* (1997a, 1997b) in which the energy distributions of the product ions were measured and analysed. Energy analysis of the emitted electrons in He^{2+}–CO collisions brings additional insight to the dynamics of charge exchange, and was recently examined by Sobocinski *et al* (2001). These authors observed Auger electrons from atomic dissociation fragments following the capture of the inner valence shell 3σ electron.

Another important issue is the state of the projectile ion after the collision. It is known that He^+ produced in He^{2+} electron capture is in an excited state (e.g. Ćirić *et al* (1985) and references therein). Recently, Kearns *et al* (2001) measured He^+ final-state selective cross sections in single-electron capture by He^{2+} on CO in the energy range 0.2–1 keV u^{-1}. By use of translational energy spectroscopy they determined relative cross sections for production of He^+ in the ground and excited $n = 2$ and 3 states. These data were normalized to the absolute cross sections of Ishii *et al* (1999). They showed that as the incident energy is lowered the non-radiative (capture into $n = 1$ of He^+) dissociative channel dominates. Another method for studying final projectile states was used by Juhász *et al* (2001), who measured the ratio of $He^+(2p–1s)$ (30.4 nm) and $He(1s2p–1s^2)$ (58.4 nm) emission lines resulting from He^{2+}–CO collisions in the 0.2–6 keV u^{-1} energy range.

In recent work in our laboratory, charge-exchange cross sections of H^+, He^+ and He^{2+} with H_2O and CO_2 have been measured (Greenwood *et al* 2000). This work complements these measurements with molecular CO, an important constituent of cometary atmospheres.

2. Experimental technique

The experimental set-up used for the present measurements is mounted on one of the beam lines at the JPL HCI Facility (Chutjian *et al* 1999) and is described in detail elsewhere (Greenwood *et al* 2000, 2001). For determining charge-exchange cross sections a retarding field is used for charge-state analysis of the scattered ions. A well collimated, small-diameter beam of the desired projectile ion is passed through a cell containing the target gas. After traversing the cell, the ion beam and its charge-exchanged components are separated by a retarding field. The transmitted ions are collected in a Faraday cup. Absolute cross sections are determined from the equation

$$\sigma_{q,q-j} = \frac{J_{q-j}}{NLJ_q^0} = \frac{qI_{q-j}}{NL(q-j)I_q^0} \tag{2}$$

where J_q^0 and J_{q-j} are the *particle* currents of incident A^{q+} and product $A^{(q-j)+}$ ions, respectively. In the present case A is ^{3}He, $q = 2$ and $j = 1$. I_q^0 and I_{q-j} are the corresponding measured *electrical* currents. The target density is $N = P_C/kT$ where P_C is absolute pressure of the target gas in the cell and T is the gas temperature. L is the ion path length through the target gas.

For this method to be applicable the single-collision condition must apply. A measure of this is that the attenuation σNL be much less than unity. If one assumes $\sigma = 10^{-14}$ cm^2 and $L = 6.08$ cm this gives the corresponding operating limit $N \ll 1.6 \times 10^{13}$ cm^{-3}, or $P_C \ll 0.5$ mTorr for a gas temperature of 300 K.

Ions are extracted from the 14.5 GHz electron cyclotron resonance ion source (ECRIS) and filtered by a double-focusing 90° magnet for the desired mass/charge (M/q) species. The ion beam is then steered into the charge-exchange beam line by a 45° electrostatic deflector, focused by an electrostatic einzel lens, and collimated by a set of four apertures. Hence a highly collimated beam enters the target gas cell which is 60.8 mm long. The ion feed gas used for the ECRIS was ^{3}He to avoid interference at $M/q = 2$ with background H_2^+ ions.

Unscattered ions as well as ions scattered within a narrow forward cone are transmitted through the cell and subsequently analysed by the retarding field. If the initial ion acceleration voltage is V_{acc} then the parent ions will be reflected by the same retarding potential. Ions which have captured j electrons will be reflected by a higher potential $V_R = V_j = qV_{acc}/(q-j)$. Therefore, the ion current has a stepwise dependence on retarding field. This allows sequential filtering of ions of decreasing charge. The height of the current step at V_j is equal to the ion current I_{q-j}.

The target density is determined by measuring the absolute target pressure P_B at a nearby capacitance manometer. The cell-gas temperature is assumed to be equal to room temperature. The measured pressure is corrected for the pressure drop between the gauge head and gas cell by calculating the duct conductance. It was verified by calibration measurements at several gas-cell conductances. The pressure correction factor PCF $= P_C/P_B$ is 0.71 and 0.60 for the two sizes of the target cell exit orifice used (see below).

Chemically pure (99.5%) CO was used throughout the measurements. It was handled with due care (CO detectors in the laboratory, and pumps vented to the roof). The base vacuum was $\approx 7 \times 10^{-9}$ Torr and was not found to contribute to the measured signals.

Two procedures are used for cross-section determination. In the first the target gas is introduced and maintained at a stable low pressure in the cell, and the ion current is measured for different retarding fields. The electrometer zero and capacitance-manometer zero must also be stable and well determined since the pressure and ion currents are at the lower limits of instrument sensitivity. When the currents and pressure are determined the cross section is

calculated using equation (2). In the second procedure the ion current variation is recorded along with the target gas pressure at various retarding potentials. In this way

(a) the linearity of signal with pressure provides a check of the single-collision condition,
(b) the incident ion current is determined from the low-pressure limit of low retarding field data, and
(c) the electrometer zero is determined from the low-pressure limit for high retarding field data.

The slope of charge-exchanged ion current versus pressure obtained with the high retarding field is directly proportional to the cross section.

This latter procedure also allows one to determine double charge-exchange cross sections for He^{2+}. The incident ion attenuation is produced by both single exchange to give singly charged He^{+} ion and double charge exchange to give neutral He°. The contribution of He^{+} to the low V_R ion–current attenuation is separately determined from measurement with a high retarding field. For $V_R > 2V_{acc}$ no ions can reach the Faraday cup. Under these conditions only fast neutral atoms traverse the retarding field, and zero current is measured.

Finally, using this procedure one can also determine the electron-capture cross section in singly charged ions (here H^{+}) assuming that beam attenuation in the target gas cell is produced only by the $q = 1 \rightarrow 0$ transition.

An example of ion current variation with pressure for a 14 keV He^{2+} incident ion beam is shown in figure 1. For a 5 kV retarding potential all ions are transmitted by the retarding barrier (curve (a)). The current attenuation arises from both production of He^{+} by single charge exchange, and from production of neutral He *via* double charge-exchange. When the retarding potential is raised to $V_R = 8$ kV (curve (b)), parent He^{2+} ions are stopped and the measured current is due to He^{+} alone. At the highest potential $V_R = 15$ kV (curve (c)) all ions are stopped: this plot serves as another check of the electrometer zero. During this test, a negative current was detected, and was traced to secondary electrons created by transmitted, metastable neutrals. Their effect on the measured current was eliminated by negatively biasing a shield electrode in front of the ion Faraday cup. The Faraday cup itself is held at ground potential, and efficient ion collection is assured by its large depth to width ratio ($6/0.4 = 15$).

The ion energy is qV_{acc} and is accurate up to the plasma potential in the ECRIS. The retarding potential current cut-off indicates that the error in this energy is about $0.05 \times q$ keV.

2.1. Measurement error

The components of the total absolute error in the measured cross sections (Greenwood *et al* 2001) are

(i) errors in current, target density and path-length determination,
(ii) statistical errors of individual measurements, and
(iii) possible systematic errors.

The present method relies on measurement of current ratios. These currents are measured with the same instrument and most often on the same measurement range. This tends to minimize errors in determined current ratios to below 1%. The error in gas-density determination arises from the instrumental accuracy (MKS Baratron, Type 627A and computer interface) (0.3%), the pressure-correction factor (2%) and the gas temperature uncertainty (0.7%). These errors combined in quadrature give a total error in the gas density determination of 2.2%. Assuming negligible background pressure the target pathlength is taken as the geometrical length L_G of the target gas cell, assuming a homogeneous gas density within

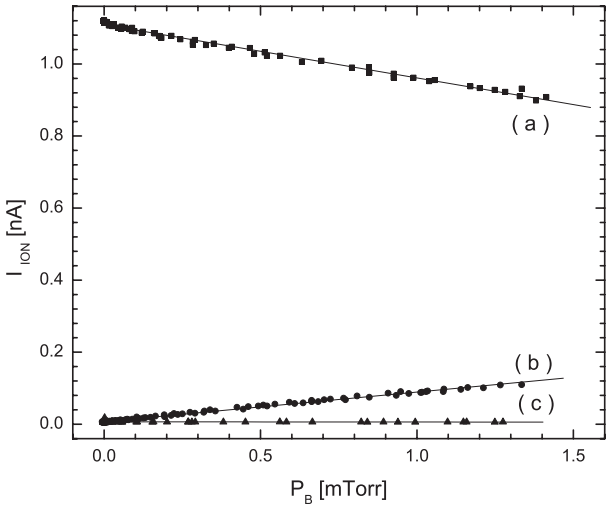

Figure 1. Ion current variation with target CO pressure for different values of retarding potential. Contributing to curve (a) are the parent He^{2+} ions and He^+ ions created by a single charge-exchange; curve (b) is the appearance of He^+ ions due to single charge-exchange; curve (c) is the result of retardation of all beams, and is a check of backgrounds and the electrometer zero. The ion acceleration voltage is 7 kV.

the cell. A lower gas density at the input and exit orifices is compensated by a longer-than-geometric path length through the gas in the vicinity outside the cell (Vane 2002). However, due to the limited pumping speed of the charge-exchange chamber some ion-background gas scattering occurs when target gas is introduced to the cell. To compensate we introduce a pathlength correction given by $L_{eff} = L_G + L_V(P_V/P_C)$, where $L_G = 6.08$ cm, L_V is the ion pathlength through the increased target background gas and P_V is background pressure as measured by a Bayard–Alpert ionization gauge. The influence of scattering on the background target gas is smaller on the charge-exchanged ion production ($L_V = 8$ cm) than on the parent-ion attenuation ($L_V = 27$ cm). Taking this into account one gets $L_{eff} = 6.18$ and 6.40 cm, respectively. The estimated error in the L determination is about 2%. Combined uncertainties lead to an error in the charge-exchange cross section of 5.2% at the 95% (2σ) confidence level.

The main sources of error in determination of the single charge-exchange cross sections are fluctuations in the ion beam current and slight variations in the beam itself due to minor day-to-day differences in the tuning conditions of the ion-transport optics. These statistical fluctuations are about 8%. Hence the total estimated error in the single charge-exchange cross sections is approximately 10% (2σ).

A larger error is encountered in the determination of the double charge-exchange cross sections. Besides the error in the single charge-exchange cross section, one has the error in an additional current-attenuation measurement. This statistical error leads to total errors averaging 17% (2σ).

One possible source of systematic error is the incomplete collection of scattered ions due to the size of the target cell exit orifice, characteristics of the retarding field configuration and the Faraday cup construction. In previous measurements of helium and proton charge-exchange cross sections in H_2O and CO_2 (Greenwood *et al* 2000) it was shown that measured cross sections were independent of exit-orifice diameter for a sufficiently large diameter. Present measurements were performed with two different exit orifices, 2.54 mm being the largest used by Greenwood *et al* (2000), and 4.09 mm in diameter. The smaller one allowed transmission of

Table 1. Single charge-exchange cross sections σ_{21} for $^3He^{2+}$ on CO.

E_{ion} (keV)	E_{ion} M^{-1} (keV u^{-1})	v_{ion} (km s^{-1})	$\sigma_{2,1}$ (10^{-16} cm^2)
1.0	0.333	254	3.2 ± 0.3
2.0	0.667	359	3.6 ± 0.3
3.0	1.000	439	4.4 ± 0.3
4.0	1.333	507	5.1 ± 0.6
5.0	1.667	567	5.4 ± 0.6
6.0	2.000	621	6.5 ± 0.7
8.0	2.667	717	7.7 ± 0.7
10.0	3.333	802	8.7 ± 0.9
12.0	4.000	879	9.9 ± 1.0
14.0	4.667	949	10.5 ± 1.1

all ions scattered within 1.2° from the centre of the entrance orifice, while this cut-off angle was 1.9° for the larger one. For these two experimental arrangements, the collimated incident beam had an angular divergence $< \pm 0.5°$ and 0.7 mm in diameter, with $\pm 0.8°$ and 1.3 mm values in the latter case. Our present experimental results and measurements of differential cross sections for similar cases (Martin *et al* (1991)—He^{2+} on D_2, O_2 and N_2; Gao *et al* (1990)—He^+ and H^+ on several gases, including CO) indicate that this effect is negligible in the present arrangement at the energies studied. A more detailed treatment of the influence of acceptance cut-off angle on the measured cross sections will be given elsewhere (Mawhorter *et al* 2002).

We point out that in the ion–molecule collisions studied (equation (1)) the product ions can be in excited states, including excited autoionizing states. In order to interpret the measured cross sections one should consider the effect of autoionizing channels on the detected currents. In the present case only He has autoionizing states, formed by double electron capture in He^{2+}. Typical flight times from the centre of the target gas cell to the Faraday cup range between 0.25 and 0.94 μs for incident energies between 14 and 1 keV, respectively. Therefore short-lived autoionizing He states would contribute to the single charge-exchange cross section, while long-lived states would be included in the double charge-exchange cross section.

3. Results and discussion

He^{2+} single and double charge-exchange measurements. Measured absolute single charge-exchange cross sections for He^{2+} on CO are presented in table 1 and figure 2. Also shown in figure 2 are the earlier data of Ishii *et al* (1999), Rudd *et al* (1985) and Shah and Gilbody (1990). Shah and Gilbody normalized their cross sections to data of Rudd *et al* (1983) for H^+–CO. Both the electron-capture cross section and the sum of electron-capture and transfer-ionization cross sections of Shah and Gilbody are shown in the figure. Present data show a steady cross-section increase with energy in the studied energy range. The cross sections of Ishii *et al* have an estimated error of $\leqslant 30\%$ so that the present cross sections are just lower than theirs even taking combined errors into account. At the higher-energy side the present data are in agreement with the data of Rudd *et al* (1985), within combined accuracies.

Double charge-exchange cross sections for He^{2+} on CO are presented in table 2 and shown in figure 3. The data of Ishii *et al* (1999) and Rudd *et al* (1985) are also shown. Present data match well with those of Ishii *et al* (1999). On the high-energy side, the present cross sections agree with those of Rudd *et al*, which show a trend of decreasing cross section with increasing energy. As one indicator of the slightly different shapes of cross sections, for the present data the cross sections for single and double-charge exchange are equal (about 4.6×10^{-16} cm^2) at

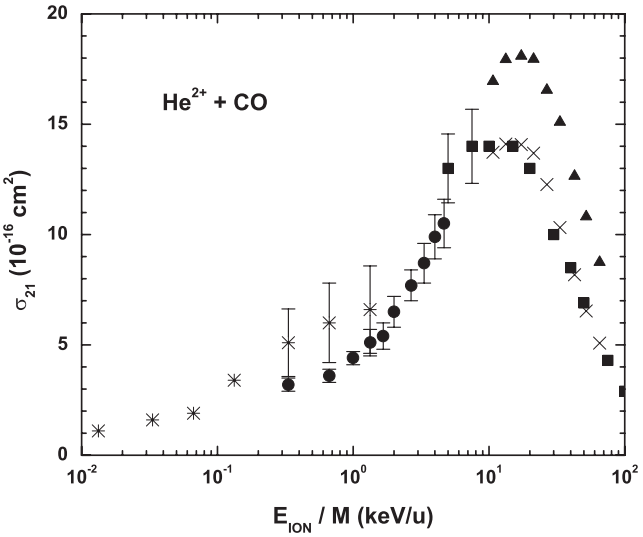

Figure 2. Measured single charge-exchange cross sections for $^3He^{2+}$ on CO. (●), present data. Other data are: Ishii *et al* (1999) (*); Rudd *et al* (1985) (■); Shah and Gilbody (1990) (×), electron capture; Shah and Gilbody (1990) (▲), the sum of electron capture and transfer ionization.

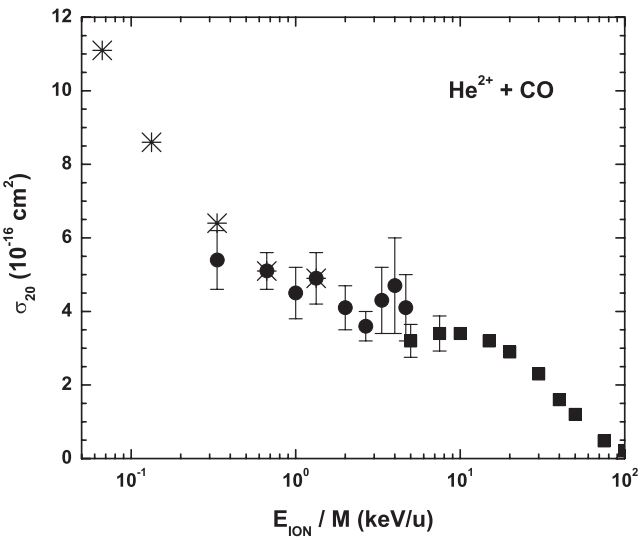

Figure 3. Measured double charge-exchange cross sections for $^3He^{2+}$ on CO. ●, present data. Other data are: Ishii *et al* (1999) (*); Rudd *et al* (1985) (■).

about 1.1 keV u^{-1}; while this happens at 0.53 keV u^{-1} with a cross section of 5.6×10^{-16} cm^2 in Ishii *et al*.

Even the simple projectile He^{2+} appears capable of exciting numerous processes when colliding with molecules. Given the high ionization and excitation energies of helium, the various transfer ionization channels (dissociative and nondissociative) and single and double electron capture channels are exothermic. Hence, due to the position of its reaction window, double charge-exchange is a dominant process at low energy (Folkerts *et al* 1997b). Excitation of autoionizing states of CO also leads to the formation of triply ionized species (Folkerts

Table 2. Double charge-exchange cross sections σ_{20} for $^3He^{2+}$ on CO.

E_{ion} (keV)	E_{ion} M^{-1} (keV u^{-1})	v_{ion} (km s^{-1})	$\sigma_{2,0}$ (10^{-16} cm^2)
1.0	0.333	254	5.4 ± 0.8
2.0	0.667	359	5.1 ± 0.5
3.0	1.000	439	4.5 ± 0.7
4.0	1.333	507	4.9 ± 0.7
6.0	2.000	621	4.1 ± 0.6
8.0	2.667	717	3.6 ± 0.4
10.0	3.333	802	4.3 ± 0.9
12.0	4.000	879	4.7 ± 1.3
14.0	4.667	949	4.1 ± 0.9

Table 3. Single charge-exchange cross sections σ_{10} for H^+ on CO.

E_{ion} (keV)	v_{ion} (km s^{-1})	$\sigma_{1,0}$ (10^{-16} cm^2)
2.5	695	13.2 ± 3
3.0	761	14.6 ± 1.4
4.0	879	14.7 ± 1.2
5.0	982	13.8 ± 1.0
6.0	1076	13.6 ± 0.9
7.0	1162	12.8 ± 0.8

et al 1997a). Recent measurements of the intensity ratio of He^+(2p–1s) and He(1s2p–1s^2) emission lines by Juhász *et al* (2001) show that this ratio increases from 2 to 30 for incident energies of 1–5 keV u^{-1}, respectively. This is consistent with the increase of the single to double charge-exchange cross section discussed above. In the present results the ratio of the single to double charge exchange cross sections varies from 1 to about 2.8 in the same energy interval. Detailed evaluation of the relationship between the cross-section ratio and the emission intensity ratio requires knowledge of the production probability (branching ratios) for the optically observed excited states.

H^+ single charge-exchange measurements. Absolute electron-capture cross sections for protons on CO are presented in table 3, and shown in figure 4 together with other data.

The electron-capture cross sections of Rudd *et al* (1983) are shown at the higher energies. These authors defined the capture cross section as the difference between measured absolute positive and negative charge-production cross sections. They used a model equation and fitted experimental data by adjusting six parameters. The resulting analytic fit is shown in figure 4. Shah and Gilbody (1990) measured separately nondissociative and dissociative channels for both electron capture and transfer ionization. At the lowest energy (13 keV), nondissociative electron capture was found to dominate (about 70%), while other capture channels and nondissociative transfer ionization made up the rest. The sum of capture and transfer ionization channels, both of which lead to production of neutral H, are also shown in figure 4. Shah and Gilbody normalized the sum of ion producing channels (direct ionization in addition to the dissociative and nondissociative channels) to the absolute ion-production cross section of Rudd *et al* (1983). They obtained partial cross sections with an estimated uncertainty of 15%. The present data agree in absolute value with those of Rudd *et al* (1983) but we observe a broad plateau in the cross section near 4 keV, whereas their parametrized model predicts a maximum at about 8 keV.

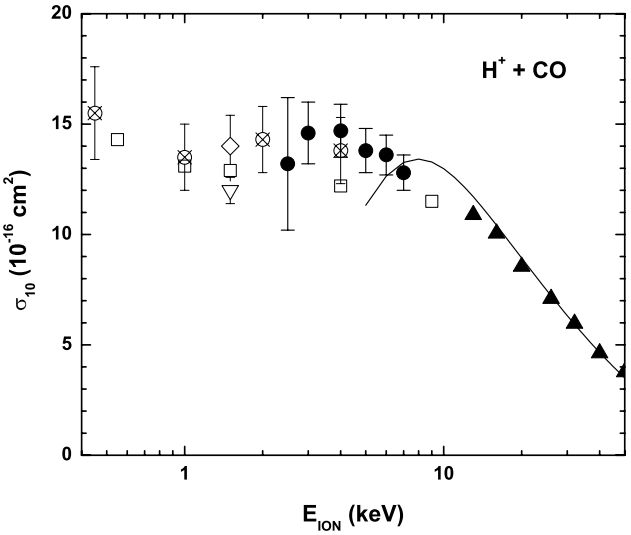

Figure 4. Measured single charge-exchange cross sections for H^+ on CO. (●), present data. Other data are: McNeal (1970) (◇); Rudd *et al* (1983) (——), parametrized fit to experimental data; Gao *et al* (1990) (▽); Shah and Gilbody (1990) (▲); Kusakabe *et al* (2000) (⊗); Kimura *et al* 2000 (□), results of an *ab initio* calculation.

On the low-energy side, the integrated angular differential cross section at 1.5 keV of Gao *et al* (1990) is shown in figure 4. Also shown is the absolute total cross section of McNeal (1970) at the same energy. The trend of our data fits nicely with these lower-energy data points. More recently, Kusakabe *et al* (2000) measured charge-transfer processes in proton collisions with molecules, including CO, in the energy range 0.2–4 keV. Their results (figure 4) show a broad plateau at energies below 4 keV. Absolute values of the present data also agree, within combined errors.

Finally, *ab initio* calculations of the H^+ + CO system have been reported by Kimura *et al* (2000). These calculations take into consideration three molecular configurations for the H^+ approach to the CO: perpendicular to the CO axis, into the C end, and into the O end. This study showed an important steric effect on the cross section. The integrated results are shown in figure 4. In particular, the theory shows a broad plateau in cross section, with no strong maximum, and is in good agreement with the experiments.

The present measurements of He^{2+} and H^+–CO charge-exchange cross sections provide needed data for modelling the interaction of the main components of the solar wind with dense neutral objects. Such objects include comets as they approach the Sun; the solar wind as it interacts with the neutral atmospheres of Venus, Earth, Mars, Jupiter and Saturn; and stellar winds as they interact with circumstellar clouds. Given the high x-ray energy and spatial resolutions of *Chandra* and *XMM–Newton* these data, and also single and multiple charge-exchange results for the minor solar-wind components which produce x-rays, provide an important part of this database.

Acknowledgments

I Čadež, M Niimura and R J Mawhorter all thank the National Research Council for Senior NRC fellowships through the NASA/NRC program. This work was carried out at the Jet Propulsion Laboratory, California Institute of Technology, and was supported through agreement with the National Aeronautics and Space Administration.

References

Chutjian A, Greenwood J B and Smith S J 1999 *Applications of Accelerators in Research and Industry (AIP Conf. Proc. vol 475)* ed J L Duggan and I L Morgan (New York: AIP)
Ćirić D, Dijkkamp D, Vlieg E and de Heer F J 1985 *J. Phys. B: At. Mol. Phys.* **18** 4745
Folkerts H O, Bliek F W, de Jong M C, Hoekstra R and Morgenstern R 1997a *J. Phys. B: At. Mol. Opt. Phys.* **30** 5833
Folkerts H O, Schlathölter T, Hoekstra R and Morgenstern R 1997b *J. Phys. B: At. Mol. Opt. Phys.* **30** 5849
Gao R S, Johnson L K, Hakes C L, Smith K A and Stebbings R F 1990 *Phys. Rev.* A **41** 5929
Greenwood J B, Chutjian A and Smith S J 2000 *Astrophys. J.* **529** 605
Greenwood J B, Williams I D, Smith S J and Chutjian A 2001 *Phys. Rev.* A **63** 062707
Ishii K, Okuno K and Kobayashi N 1999 *Phys. Scr.* T **80** 176
Juhász Z, Lubinski G, Morgenstern R and Hoekstra R 2001 *22nd Int. Conf. on Photon, Electron and Atom Collisions—Contributed Papers (Santa Fe, NM, USA, July 2001)* ed S Datz *et al* (Princeton, NJ: Rinton Press) p 590
Kearns D M, Gillen D R, Voulot D, Greenwood J B, McCullough R W and Gilbody H B 2001 *J. Phys. B: At. Mol. Opt. Phys.* **34** 3401
Kimura M, Gu J-P, Hirsch G, Buenker R J and Stancil P C 2000 *Phys. Rev.* A **61** 032708
Krasnoplosky V A and Mumma M J 2001 *Astrophys. J.* **549** 629
Kusakabe T, Asahina K, Gu J P, Hirsch G, Buenker R J, Kimura M, Tawara H and Nakai Y 2000 *Phys. Rev.* A **62** 062714
Magnani L and A'Hearn M F 1986 *Astrophys. J.* **302** 477
Martin S J, Stevens J and Pollack E 1991 *Phys. Rev.* A **43** 3503
Mawhorter *et al* 2002 at press
McNeal R J 1970 *J. Chem. Phys.* **53** 4308
Rudd M E, DuBois R D, Toburen L H, Ratcliffe C A and Goffe T V 1983 *Phys. Rev.* A **28** 3244
Rudd M E, Goffe T V and Itoh A 1985 *Phys. Rev.* A **32** 2128
Schwadron N A and Cravens T E 2000 *Astrophys. J.* **544** 558
Shah M B and Gilbody H B 1990 *J. Phys. B: At. Mol. Opt. Phys.* **23** 1491
Sobocinski P, Rangama J, Chesnel J-Y, Tarisien M, Adoui L, Cassimi A, Husson X and Frémont F 2001 *J. Phys. B: At. Mol. Opt. Phys.* **34** L367
Tosh R E and Johnsen R 1993 *Int. J. Mass Spectrom. Ion Process.* **123** 193
Vane C R 2002 private communication